Yoon *et al. Respiratory Research* (2026) 27:409
https://doi.org/10.1186/s12931-026-03834-9

Respiratory Research

RESEARCH Open Access

PRL-3–sensitive cytoskeletal signaling mediates early airway epithelial responses to particulate matter

Hyungkyung Yoon[1†], Moonhwan Choi[1†], Youngeun Ha[1], Jiwon An[1], An-Soo Jang[2], Sang-Kyung Lee[1] and Taiyoun Rhim[1,3*]

Abstract

Background Airborne particulate matter is a major environmental risk factor for airway disease, but the early molecular events that initiate epithelial dysfunction before overt inflammation remain poorly understood. In particular, the mechanisms by which acute, non-cytotoxic particulate exposure disrupts epithelial structural organization have not been fully defined.

Methods We used an unbiased phosphoproteomic approach to identify early signaling responses in human bronchial epithelial cells exposed to particulate matter under non-lethal conditions. Phosphatase of regenerating liver-3 (PRL-3; gene symbol PTP4A3) function was evaluated using pharmacologic inhibition and genetic suppression, with in vivo validation in a mouse acute airway exposure model. Data were analyzed using appropriate parametric or non-parametric tests, including one-way or two-way analysis of variance, and P values < 0.05 were considered statistically significant.

Results Phosphoproteomic profiling identified coordinated changes in cytoskeleton-associated proteins, including ezrin-radixin-moesin family members, suggesting early disruption of membrane-cytoskeleton coupling after particulate exposure. Acute particulate exposure induced rapid and transient upregulation and membrane relocalization of PRL-3, accompanied by PRL-3-sensitive ezrin dephosphorylation in vitro and in vivo. Pharmacological inhibition or genetic suppression of PRL-3 restored ezrin phosphorylation and attenuated epithelial–mesenchymal transition (EMT)-associated molecular changes and mucin 5AC (MUC5AC) upregulation. These effects were observed independently of protein kinase B (Akt), extracellular signal-regulated kinase (ERK), and mechanistic target of rapamycin (mTOR) signaling, and were reproducible across multiple particulate types, including urban particulate matter (UPM), diesel exhaust particles (DEP), and particulate matter with an aerodynamic diameter of ≤ 10 μm (PM_{10}).

†Hyungkyung Yoon and Moonhwan Choi contributed equally to the work.

*Correspondence:
Taiyoun Rhim
rhim@hanyang.ac.kr

Full list of author information is available at the end of the article

© The Author(s) 2026. **Open Access** This article is licensed under a Creative Commons Attribution-NonCommercial-NoDerivatives 4.0 International License, which permits any non-commercial use, sharing, distribution and reproduction in any medium or format, as long as you give appropriate credit to the original author(s) and the source, provide a link to the Creative Commons licence, and indicate if you modified the licensed material. You do not have permission under this licence to share adapted material derived from this article or parts of it. The images or other third party material in this article are included in the article's Creative Commons licence, unless indicated otherwise in a credit line to the material. If material is not included in the article's Creative Commons licence and your intended use is not permitted by statutory regulation or exceeds the permitted use, you will need to obtain permission directly from the copyright holder. To view a copy of this licence, visit http://creativecommons.org/licenses/by-nc-nd/4.0/.

Conclusions Our findings identify a PRL-3-sensitive, cytoskeleton-centered signaling pathway as an early molecular mechanism connecting particulate exposure to molecular alterations associated with early airway epithelial responses.

Keywords Particulate matter, PRL-3 (PTP4A3), Ezrin dephosphorylation, Mucin overproduction, Phosphoproteomics

Background

Airborne particulate matter (PM) is a major environmental pollutant that contributes to the development and exacerbation of airway diseases [1, 2]. As the first point of contact for inhaled particles, the airway epithelium plays a central role in maintaining barrier integrity, mucociliary clearance, and immune homeostasis [3, 4]. Accordingly, disruption of epithelial structure and function is considered an early and critical event in PM-induced airway pathology [5].

Previous studies have shown that PM exposure promotes oxidative stress, inflammatory signaling, and mucin overproduction in airway epithelial cells [6–8]. However, these responses largely reflect downstream consequences of exposure and do not fully explain how epithelial dysfunction is initiated immediately after particle contact. In particular, the early intracellular signaling mechanisms that precede overt cytotoxicity and inflammation remain poorly defined [9]. Acute high-level particulate exposure may occur during wildfire smoke episodes, severe air pollution events, industrial accidents, or occupational inhalation of particle-rich aerosols [10, 11]. Under these conditions, airway epithelial cells can encounter a high particulate burden over a short period, making early non-cytotoxic signaling responses relevant to the initiation of epithelial alterations.

Increasing evidence suggests that epithelial structural integrity is highly sensitive to environmental stress and that cytoskeleton-associated signaling pathways may act as early responders to particulate exposure [12–14]. Among the key regulators of epithelial architecture are the ezrin-radixin-moesin (ERM) proteins, which mediate membrane-cytoskeleton coupling and are essential for maintaining cell shape, polarity, and regulated secretion [15, 16]. Despite their importance in epithelial homeostasis, the molecular events linking particulate exposure to early cytoskeletal disruption have not been systematically characterized.

Because cytoskeletal organization is tightly regulated by phosphorylation-dependent signaling, phosphoproteomic analysis provides a useful strategy for identifying early molecular responses to particulate exposure [17, 18]. Phosphatase of regenerating liver-3 (PRL-3; gene symbol PTP4A3), a protein tyrosine phosphatase, has been implicated in cytoskeletal regulation, membrane dynamics, and epithelial plasticity [19–21]. However, its role in non-malignant airway epithelial cells, particularly in the context of environmental particulate exposure, is unknown.

In the present study, we combined an unbiased phosphoproteomic approach with targeted validation and in vivo analyses to define early signaling mechanisms associated with particulate-induced changes in airway epithelial structure. To investigate particle-induced signaling under controlled, non-lethal conditions, we used titanium dioxide (TiO_2) as a defined model particle. We identify PRL-3 as a previously unrecognized early signaling mediator associated with particulate-induced ezrin dephosphorylation, epithelial–mesenchymal transition (EMT)-associated molecular changes, and mucin 5AC (MUC5AC) upregulation.

Materials and methods

Cell culture

Human bronchial epithelial cells (BEAS-2B) were cultured in Dulbecco's Modified Eagle Medium (DMEM) according to the manufacturer's instructions. Cells were maintained at 37 °C in a humidified atmosphere containing 5% CO_2 and used between passages 5 and 20. All cell lines were authenticated by short tandem repeat profiling and routinely tested to confirm the absence of Mycoplasma contamination.

Particulate matter (PM) preparation and treatment

Titanium dioxide (TiO_2) particles were used as a compositionally defined model particulate system to investigate early molecular signaling responses to particulate exposure under controlled experimental conditions. TiO_2 was selected to reduce the chemical heterogeneity inherent to ambient particulate matter and to enable focused analysis of particle-associated cytoskeletal signaling. Prior to cell exposure, particles were suspended in serum-free medium and sonicated immediately before use to minimize aggregation.

Cells were exposed to TiO_2 particles at concentrations ranging from 0.4 to 100 μg/mL for the indicated time periods. These concentrations were selected to examine dose-dependent cellular responses and to capture early signaling events following acute particulate exposure. This experimental system was designed to model molecular initiating events rather than to fully recapitulate chronic environmental inhalation exposure.

To reduce potential endotoxin contamination, TiO_2 particles were heat-treated at 180 °C for 8 h prior to use. Although this procedure substantially reduces endotoxin

levels, residual contamination could not be completely excluded and is considered a limitation of the experimental model.

The urban particulate matter (UPM), diesel exhaust particles (DEP), and particulate matter with an aerodynamic diameter of ≤ 10 μm (PM_{10}) were also suspended in DMEM. Prior to exposure, all suspensions were thoroughly mixed by repeated pipetting (20–30 times) and gentle vortexing to minimize aggregation and ensure a uniform dispersion. No dispersing agents were used. For PM treatment, BEAS-2B cells were seeded in T-75 cell culture flasks at 2.0×10^5 cells/mL and cultured for 24 h. Cells were then treated with 0.4, 4, 40, or 100 μg/mL TiO_2 particles, 100 μg/mL UPM [22, 23], DEP [24, 25], or PM_{10} [26, 27] and incubated at 37℃ for 1 h.

Inhibitor treatment

PRL-3 inhibitor I (Sigma Aldrich), Akt inhibitor VIII (Merck, Darmstadt, Germany), ERK inhibitor (PD98059) (Cell Signaling Technology, Danvers, MA, USA), and mTOR inhibitor (KU-0063794) (Sigma Aldrich) were dissolved in dimethyl sulfoxide (DMSO). For inhibitor treatments, BEAS-2B cells were seeded as described above, pre-treated with inhibitors at a final concentration of 5 μM for 1 h, and treated with 100 μg/mL TiO_2 particles for an additional 1 h at 37℃.

RNA interference (siRNA Transfection)

PRL-3-specific small interfering RNA (siRNA) (sense: 5'-TCT CGT TTC TCT TGG ACA A-3') was synthesized as previously described [28]. For siRNA transfection, BEAS-2B cells were seeded in T-75 cell culture flasks (2.0×10^5 cells/mL) and cultured in DMEM supplemented with 10% heat-inactivated fetal bovine serum (FBS) and 100 units/ml penicillin for 24 h. PRL-3 siRNA was transfected at a final concentration of 90 nM using a commercial transfection reagent. Following transfection, cells were incubated for 12 h at 37℃ in a humidified 5% CO_2 incubator before treatment with 4 μg/mL TiO_2 or silicon dioxide (SiO_2) particles for 1 h.

Cell viability assay (WST-1)

Cell viability was measured using the EZ-Cytox enhanced cell viability assay kit (DoGenBio, Seoul, Korea). BEAS-2B cells were seeded in 96-well plates at densities of 4.0×10^4 cells/well and 5.0×10^3 cells/well for 1-hour and 72-hour treatments, respectively, and incubated for 24 h at 37℃. Cells were then treated with 0.4, 4, 40, or 100 μg/mL of TiO_2 particles for the specified durations. After TiO_2 exposure, cells were washed and the medium was replaced with fresh culture medium before WST-1 reagent addition. To reduce the influence of residual TiO_2-associated turbidity or background absorbance, absorbance was measured in each well immediately before adding the WST-1 reagent. WST-1 assay reagent was added to the culture medium at a 1:10 dilution. After a 1-hour incubation at 37℃, absorbance was measured at 450 nm using a microplate reader (Molecular Devices, San Jose, CA, USA). The pre-WST-1 absorbance value was subtracted from the post-WST-1 absorbance value for each corresponding well, and the corrected absorbance values were used to calculate relative cell viability.

Phosphoproteomic analysis

For phosphoproteomic profiling, cells were harvested following acute particulate exposure and lysed in phosphatase inhibitor–containing buffer. Protein extracts were subjected to tryptic digestion, phosphopeptide enrichment, and liquid chromatography–tandem mass spectrometry (LC–MS/MS) analysis as previously described [29, 30]. Phosphorylation changes were quantified using label-free approaches, and differentially regulated phosphosites were identified based on reproducible changes across three independent experiments. Detailed mass spectrometry procedures, quality control parameters, and data processing pipelines are provided in Additional file 1.

Western blot analysis

Cellular extracts from treated BEAS-2B cells (as described in PM treatment and inhibitor/siRNA sections) were obtained using RIPA buffer. Protein concentrations were quantified using a BCA assay kit. Samples were separated on 10% sodium dodecyl sulphate polyacrylamide gels and transferred to polyvinylidene difluoride (PVDF) membranes (Millipore, Merck, Burlington, MA, USA). Membranes were blocked with 5% skim milk at room temperature for 1 h and then incubated overnight at 4℃ with primary antibodies diluted in 5% skim milk. Primary antibodies were Ezrin (3C12) (#MA5-13862, Thermo Fisher Scientific, Waltham, MA, USA; 1:400 dilution), Ezrin (phospho T567) (ab47293, Abcam, Cambridge, UK; 1:1000 dilution), MUC5AC (ab198294, Abcam; 1:20000 dilution), PRL-3 (PA5-106905, Thermo Fisher Scientific; 1:1000 dilution), E-cadherin (#3195, Cell Signaling Technology, Danvers, MA, USA; 1:1000 dilution), Vimentin (#5741, Cell Signaling Technology; 1:1000 dilution), and β-actin (GTX109639, GeneTex, Irvine, CA, USA; 1:5000 dilution). Unbound primary antibodies were removed with 1X Tris-buffered saline (TBS) washing buffer containing 0.1% (v/v) Tween20. Membranes were then incubated with horseradish peroxidase-conjugated secondary antibodies (GTX213110-01 or GTX213111-01, GeneTex, Irvine, CA, USA; 1:2000 dilution) at room temperature for 1 h. Target proteins were detected via chemiluminescence using enhanced chemiluminescence (ECL) solution (Amersham Biosciences, Cleveland, OH, USA). Western blot band intensities were quantified by densitometric

analysis of chemiluminescent signals and normalized to β-actin.

Immunocytochemistry (ICC)

BEAS-2B cells were seeded in 8-well chamber slides at 8.0×10^3 cells/well and cultured for 48 h at 37°C. Cells were then treated with 0.4, 4, or 100 μg/mL of TiO_2 particles for 1 h. Following the treatments, cells were washed with 1X phosphate-buffered saline (PBS) and fixed with 4% paraformaldehyde for 10 min at room temperature. After fixation, permeabilization and blocking were performed simultaneously using 5% normal goat serum (NGS) containing 0.1% saponin for 1 h and then incubated with an anti-PRL-3 antibody (PA5-106905, Thermo Fisher Scientific; 1:200 dilution) diluted in antibody dilution buffer containing 2% NGS, 1% bovine serum albumin (BSA), and 0.05% saponin for 2 h. After three washes with 1X PBS, samples were incubated with a fluorescein isothiocyanate (FITC)-conjugated goat anti-rabbit IgG secondary antibody (ab6717, Abcam; 1:500) for 1 h in the dark. Cell nuclei were counterstained with 4′,6-diamidino-2-phenylindole (DAPI) (USB, Cleveland, OH, USA). All incubation steps, including blocking, primary and secondary antibody incubation, and DAPI staining, were performed at room temperature. Fluorescence images were acquired using a confocal laser scanning microscope (Zeiss LSM900, Carl Zeiss, Oberkochen, Germany).

RNA extraction and reverse transcription-PCR (RT-PCR)

Total RNA was isolated from 2.0×10^7 BEAS-2B cells using TRIzol reagent (Invitrogen, Carlsbad, CA, USA). cDNA was synthesized from 1 μg of total RNA using a SuperScript III kit (Invitrogen) and used as a template for PCR. Primer sequences used were β-actin (forward; 5'-GCA CTC TTC CAG CCT TCC TTC C-3', reverse; 5'-TCA CCT TCA CCG TTC CAG TTT TT-3'), and MUC5AC (forward; 5'-GGA GGT GCC CAC TTC TCA AC-3', reverse; 5'-CTT CAG GCA GGT CTC GCT G-3'). PCR products were separated by electrophoresis on 1.3% agarose gels and visualized using a gel documentation system (Davinch-Gel Imaging System, Davinch-K, Seoul, Korea). Band intensities of semi-quantitative RT-PCR products were quantified by densitometric analysis using ImageJ software. MUC5AC band intensity was normalized to the corresponding β-actin band intensity.

Animal model and treatments

Seven-week-old female BALB/c mice were purchased from NARA Biotech (Seoul, Korea) and housed in a specific pathogen-free (SPF) facility under controlled environmental conditions with a 12-hour light/dark cycle and ad libitum access to food and water. Female mice were selected to maintain consistency with established airway exposure protocols in our laboratory and to reduce sex-related variability within this exploratory in vivo validation experiment. All animal procedures were approved by the Institutional Animal Care and Use Committee of Hanyang University (Approval number: HY-IACUC-25-0227). Mice were randomly divided into four groups ($n = 4$): Control, TiO_2-treated, PRL-3 inhibitor-treated, and PRL-3 siRNA-treated. For tracheal instillation, mice were anaesthetized with a PBS, Zoletil, and Rumpun mixture at a 6:3:1 ratio (PBS: Zoletil: Rumpun). Group 2 received 100 μg of TiO_2 particles suspended in 100 μL LPS-free PBS (4 mg/kg). Groups 3 and 4 received 0.5 μM of PRL-3 inhibitor and PRL-3 siRNA, respectively, in 100 μL LPS-free PBS as a pretreatment. One hour after pretreatment, mice were intratracheally instilled with 100 μg TiO_2 particles suspended in 100 μL LPS-free PBS. All mice were sacrificed under anesthesia 1 h after treatment.

Tissue preparation & immunohistochemistry

Mouse lungs were perfused via the heart with LPS-free PBS to flush out red blood cells. Tissues were fixed with 4% (v/v) buffered paraformaldehyde for 24 h and embedded in paraffin. Embedded tissue Sect. (4 μm thickness) were mounted on glass slides. Section (4 μm thickness) were deparaffinized at 60℃ and rehydrated through a graded series of ethanol (100%, 90%, 80%, 70%). Samples were incubated in blocking buffer (5% normal goat serum (NGS) and 0.3% Tween20 in TBS) for 1 h at room temperature. Sections were then incubated overnight at 4℃ in a humidified chamber with primary antibodies of Ezrin (phospho T567) (Abcam, Cambridge, UK; 1:1000 dilution) and Ezrin (3C12) (Thermo Fisher Scientific, Waltham, MA, USA; 1:400 dilution) diluted in blocking buffer. Unbound primary antibodies were removed with 1X TBS washing buffer containing 0.3% (v/v) Tween20. Tissue sections were incubated with FITC-conjugated secondary antibodies (Ab Frontier, Seoul, Korea; 1:32 dilution) in a humidified chamber for 1 h at room temperature. Cell nuclei were stained with 4′,6-diamidino-2-phenylindole (DAPI) (USB, Cleveland, OH, USA). Tissue sections were examined using a fluorescence microscope (CELENA® S Digital Imaging System, Logos Biosystems, Anyang, Gyeonggi-do, Korea). Lung tissue sections containing bronchi and bronchioles were selected for analysis to assess airway epithelial responses following intratracheal instillation.

Quantification of fluorescence intensity

Fluorescence intensity was quantified using ImageJ software. For immunocytochemistry, regions of interest (ROIs) were selected to include DAPI-positive cells within each field, and PRL-3 FITC fluorescence intensity and DAPI fluorescence intensity were measured from the corresponding ROIs. For immunohistochemistry,

airway epithelial regions in bronchi and bronchioles were selected as ROIs based on tissue morphology and DAPI staining, and pEZR FITC fluorescence intensity and DAPI fluorescence intensity were measured from the corresponding epithelial ROIs. Background fluorescence was subtracted using signal measured from adjacent non-cellular regions. FITC fluorescence intensity was normalized to DAPI fluorescence intensity, and the normalized values were expressed as fold change relative to the control group. For each sample, at least three non-overlapping fields were analyzed using the same ROI selection criteria across groups. The same image acquisition settings were applied across groups within each experiment.

Statistics

Data from in vitro experiments are presented as mean ± standard deviation (SD) and were analyzed using parametric statistical methods after confirmation of normality. Comparisons among multiple groups were performed using one-way analysis of variance (ANOVA) followed by Tukey's post hoc test. Experiments involving two independent variables were analyzed using two-way ANOVA.

Data derived from in vivo experiments are presented as median with interquartile range (IQR) and were analyzed using non-parametric statistical tests. All statistical analyses were two-sided, and P values < 0.05 were considered statistically significant. Analyses were performed using GraphPad Prism (Ver.10.5.0).

Results

Phosphoproteomic profiling reveals enrichment of cytoskeleton-associated signaling proteins following acute TiO_2 exposure

To systematically identify early molecular responses under defined non-cytotoxic conditions, we first established a non-lethal exposure window for acute particulate treatment. Short-term (1 h) exposure to TiO_2 particles across a range of concentrations did not significantly affect BEAS-2B cell morphology or corrected WST-1 viability, whereas prolonged exposure (72 h) resulted in dose-dependent cytotoxicity (Additional file 2: Fig. S1A-C). These findings indicate a controlled early, non-cytotoxic time window suitable for mechanistic investigation. The 72-hour WST-1 assay was used to evaluate general cytotoxicity after prolonged exposure, whereas subsequent mechanistic analyses were performed under the 1-hour exposure condition.

Under these defined conditions, BEAS-2B cells were exposed to TiO_2 particles for 1 h and subjected to phosphoproteomic analysis. Phosphoprotein-enriched lysates were analyzed by nano–LC–MS/MS, and proteins exhibiting reproducible changes in phosphorylation status were identified (Table 1).

Table 1 Top 15 phosphoproteins showing reproducible phosphorylation changes following acute TiO_2 exposure

IPI number	Protein name	0 μ g/ml	0.4 μ g/ml	4 μ g/ml
IPI00843975 (+1)	EZR Ezrin	23	16	6
IPI00219365 (+1)	MSN Moesin	21	17	5
IPI00017367 (+1)	RDX Radixin, isoform CRA_a	20	17	5
IPI00186290	EEF2 Elongation factor 2	20	1	6
IPI00018146	YWHAQ 14-3-3 protein theta	22	17	13
IPI00017334	PHB Prohibitin	8	3	0
IPI00216135	TPM1 Isoform 3 of Tropomyosin alpha-1 chain	7	0	0
IPI00299155 (+1)	PSMA4 Proteasome subunit alpha type-4	5	2	0
IPI00783271	LRPPRC Leucine-rich PPR motif-containing protein, mitochondrial	5	4	0
IPI00291175 (+1)	VCL Isoform 1 of Vinculin	6	4	1
IPI00016832 (+1)	PSMA1 Isoform Short of Proteasome subunit alpha type-1	8	6	3
IPI00216318	YWHAB Isoform Long of 14-3-3 protein beta/alpha	22	21	17
IPI00456969	DYNC1H1 Cytoplasmic dynein 1 heavy chain 1	4	0	0
IPI00018352	UCHL1 Ubiquitin carboxyl-terminal hydrolase isozyme L1	4	1	0
IPI00024175	PSMA7 Isoform 1 of Proteasome subunit alpha type-7	5	0	1

Proteins were identified by nano–LC–MS/MS analysis of phosphoprotein-enriched lysates from BEAS-2B cells treated with TiO_2 particles for 1 h under non-cytotoxic conditions. Among approximately 200 detected phosphoproteins, the top 15 proteins exhibiting consistent phosphorylation changes across independent experiments are presented. Reproducibility was evaluated using three independent experiments. Ezrin, which was further examined in subsequent functional analyses, is indicated

Proteomic discovery experiments were conducted at low, non-cytotoxic concentrations (0.4–4 μg/mL) to capture early signaling events, whereas selected validation experiments employed higher concentrations (up to 100 μg/mL) within the established non-lethal exposure window to confirm robustness of the observed signaling responses

Among approximately 200 detected phosphoproteins, proteins associated with membrane–cytoskeleton coupling and cytoskeletal regulation were prominently enriched following acute TiO_2 exposure. Notably, all three members of the ERM family—ezrin (EZR), moesin (MSN), and radixin (RDX)—exhibited reproducible phosphorylation changes. Additional cytoskeletal and mechanical components, including vinculin (VCL), tropomyosin 1 (TPM1), and cytoplasmic dynein heavy chain 1 (DYNC1H1), were also identified. Proteins involved in signal scaffolding (YWHAQ and YWHAB) and cellular stress or proteostasis (EEF2, PHB, UCHL1, and PSMA subunits) were concurrently detected.

This phosphoproteomic signature indicated that acute particulate exposure preferentially engages cytoskeleton-associated signaling networks rather than inducing generalized cytotoxic responses. Based on the central role of ERM proteins in epithelial structure and the known ability of protein tyrosine phosphatase PRL-3 to regulate ezrin phosphorylation [28], subsequent analyses focused on the PRL-3–ERM signaling axis. Consistent with the phosphoproteomic enrichment of ERM family members, acute TiO_2 exposure also induced phosphorylation changes in moesin and radixin in vivo, as demonstrated in lung tissue sections from TiO_2-instilled mice (Additional file 2: Fig. S2A, B).

TiO_2 particles induce rapid ezrin dephosphorylation in vitro and in vivo

Guided by the phosphoproteomic findings (Table 1), we next examined the phosphorylation status of ezrin following TiO_2 exposure. Although phosphorylation changes were detected across all ERM family members, subsequent mechanistic analyses focused on ezrin because of its established role in airway epithelial structure and epithelial secretory regulation. Time-course analysis revealed that treatment with TiO_2 (100 μg/mL) induced a rapid decrease in ezrin phosphorylation at Thr567, with significant reductions detected at 45 min (38.9%) and 60 min (45.5%) relative to untreated controls ($p < 0.05$), while total ezrin protein levels remained unchanged (Fig. 1A, B).

Dose–response analysis further demonstrated that 1-hour exposure to TiO_2 particles resulted in a concentration-dependent decrease in phosphorylated ezrin, with a significant reduction of approximately 40.1% observed at 100 μg/mL ($p < 0.05$) (Fig. 1C, D).

To assess the in vivo relevance of these findings, BALB/c mice were intratracheally instilled with TiO_2 particles, and lung tissues were examined by immunohistochemistry. Phosphorylated ezrin was markedly reduced in the bronchi and bronchioles of TiO_2-treated mice, showing a 90.7% decrease compared with control animals ($p < 0.05$) (Fig. 1E, F). These results demonstrate that TiO_2 particles rapidly induce ezrin dephosphorylation both in vitro and in vivo.

PRL-3 is functionally involved in TiO_2-induced ezrin dephosphorylation

Given the established role of PRL-3 in regulating ezrin phosphorylation and its positioning within cytoskeleton-associated signaling networks identified by phosphoproteomics, we next investigated whether PRL-3 mediates TiO_2-induced ezrin dephosphorylation. Pre-treatment of BEAS-2B cells with a PRL-3 inhibitor completely prevented the decrease in phosphorylated ezrin induced by TiO_2 exposure (Fig. 2A, B).

Consistently, genetic silencing of PRL-3 using siRNA similarly blocked ezrin dephosphorylation in response to both TiO_2 and silicon dioxide (SiO_2) particles (Fig. 2C). In vivo, pretreatment of mice with either a PRL-3 inhibitor or PRL-3 siRNA restored ezrin phosphorylation in the bronchi and bronchioles following TiO_2 exposure (Fig. 2D–G). Together, these results support PRL-3 as a phosphatase-associated regulatory mediator functionally involved in particulate-induced ezrin dephosphorylation.

TiO_2 exposure induces transient PRL-3 upregulation and membrane relocalization associated with EMT-related marker changes

To further elucidate the role of PRL-3 in particulate-induced epithelial responses, we examined changes in PRL-3 expression and subcellular localization following TiO_2 exposure. Immunocytochemical analysis revealed a rapid and transient increase in PRL-3 immunoreactivity within 10–30 min of exposure, accompanied by pronounced redistribution of PRL-3 toward the plasma membrane (Fig. 3A–G). Representative Western blot images showed an early increase in PRL-3 protein signal following TiO_2 exposure, supporting a transient PRL-3 protein response during the acute exposure period (Fig. 3H–K).

TiO_2 exposure significantly reduced expression of the epithelial marker E-cadherin (41.0% decrease, $p < 0.05$) and increased expression of the mesenchymal marker vimentin (2.45-fold increase, $p < 0.05$), indicating EMT-associated changes in marker expression under acute exposure conditions (Fig. 3L–N). PRL-3 inhibition attenuated these changes, maintaining E-cadherin expression and suppressing vimentin upregulation.

Ezrin dephosphorylation and MUC5AC upregulation occur independently of Akt, ERK, and mTOR signaling

Because MUC5AC upregulation is associated with airway mucus hypersecretion, we next examined the regulation of MUC5AC expression. Semi-quantitative RT-PCR with densitometric analysis showed that TiO_2 significantly increased the MUC5AC mRNA signal by approximately

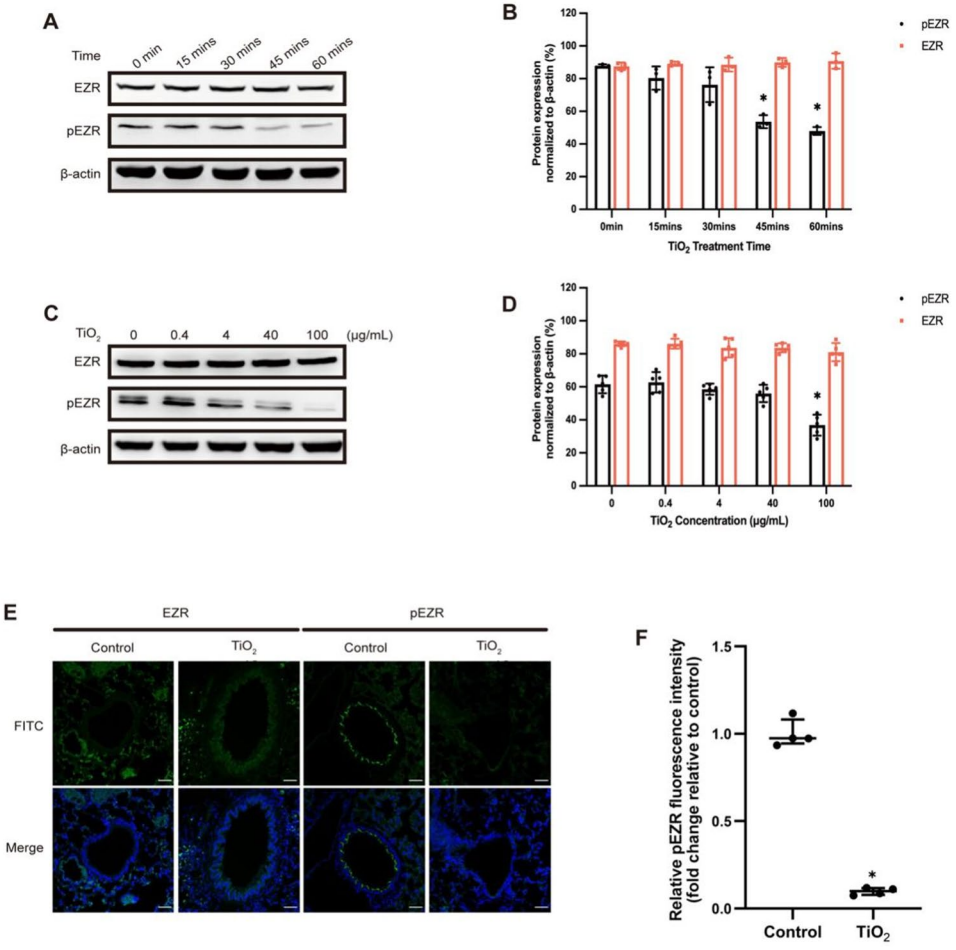

Fig. 1 Acute TiO_2 exposure induces rapid ezrin dephosphorylation under non-cytotoxic conditions. **A** Immunoblot analysis of total ezrin (EZR) and phosphorylated ezrin (pEZR, Thr567) in BEAS-2B cells treated with TiO_2 (100 μg/mL) for the indicated times. **B** Densitometric quantification of TiO_2 time-dependent changes in pEZR and total EZR levels normalized to β-actin. $n = 3$ per group. **C** Immunoblot analysis of total EZR and pEZR in BEAS-2B cells following 1-hour TiO_2 exposure at increasing concentrations. **D** Densitometric quantification of TiO_2 dose-dependent changes in pEZR and total EZR levels normalized to β-actin. $n = 5$ per group. **E** Representative immunofluorescence images of lung bronchi and bronchioles from control and TiO_2-instilled mice. EZR and pEZR were detected in separate tissue sections using fluorescein isothiocyanate (FITC)-conjugated secondary antibodies. Merged images show FITC (green) and nuclear staining with DAPI (blue). Scale bar = 20 μm. **F** Quantification of pEZR fluorescence intensity normalized to DAPI. $n = 4$ per group. Data are presented as mean ± SD for in vitro experiments, and shown as individual data points with median and interquartile range (IQR) for in vivo experiments. $^*p < 0.05$ versus respective control

2.1-fold compared with control, and this increase was attenuated by PRL-3 inhibition (Fig. 4A, B).

To determine whether classical signaling pathways contribute to this response, cells were pre-treated with inhibitors of Akt, ERK, or mTOR complexes prior to TiO_2 exposure. None of these inhibitors prevented TiO_2-induced ezrin dephosphorylation or MUC5AC upregulation (Fig. 4C–G), indicating that PRL-3-sensitive regulation of ezrin phosphorylation and MUC5AC expression occurs independently of these canonical signaling pathways.

PRL-3-sensitive ezrin dephosphorylation extends to environmentally relevant particulate matter types

To assess the generalizability of this mechanism, BEAS-2B cells were exposed to urban particulate matter (UPM), diesel exhaust particles (DEP), or PM_{10}. Each particulate type induced significant ezrin dephosphorylation, with reductions of 21.3%, 35.1%, and 15.6%, respectively ($p < 0.05$) (Fig. 5A–I).

Pre-treatment with a PRL-3 inhibitor consistently prevented ezrin dephosphorylation induced by all tested particulate types, supporting that PRL-3-sensitive ezrin dephosphorylation is observed across chemically diverse airborne particulates.

Integrated model of PRL-3-sensitive cytoskeletal signaling in particulate-induced airway epithelial responses

Collectively, these findings demonstrate that acute particulate matter exposure rapidly engages a cytoskeleton-associated signaling network identified by

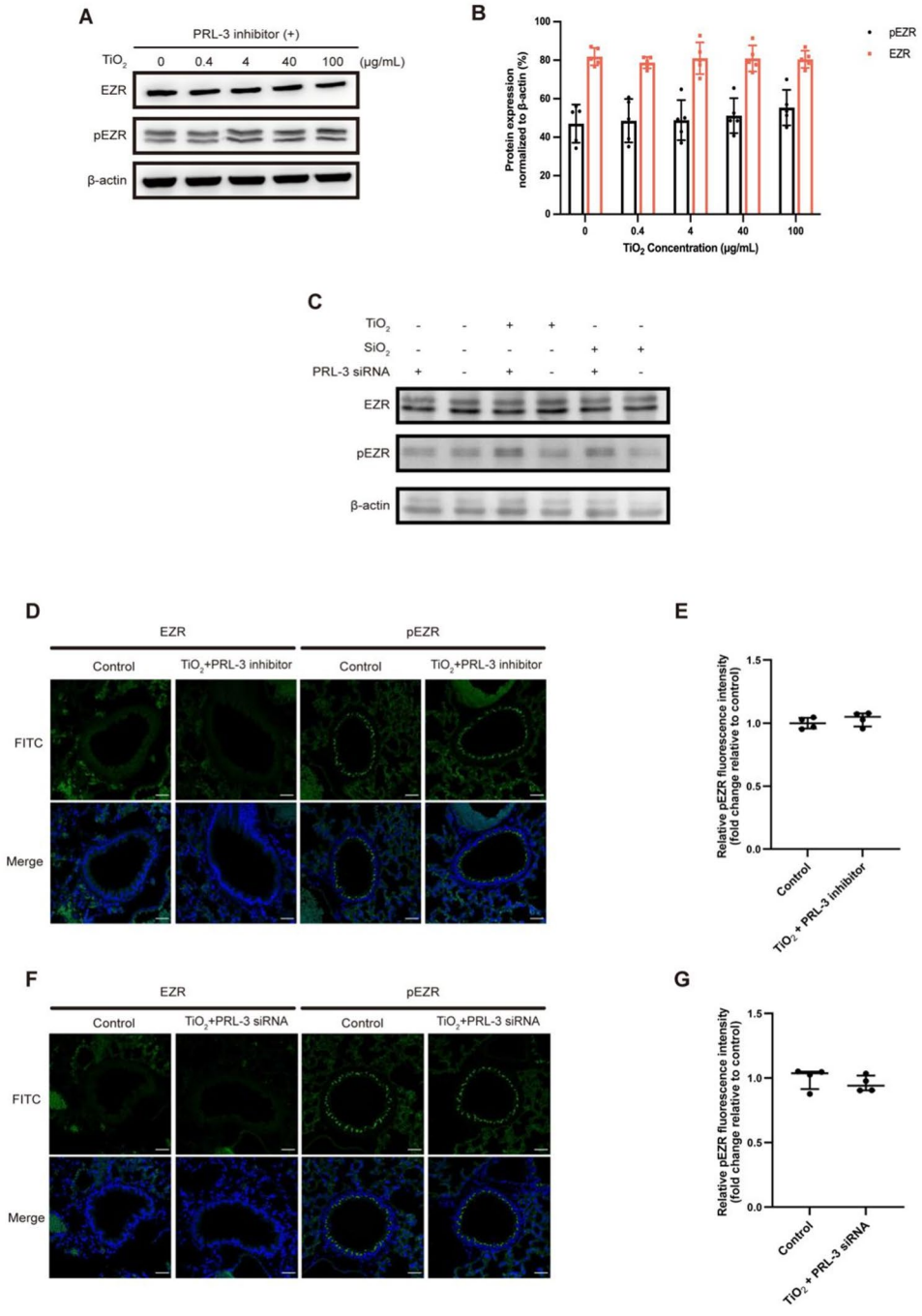

Fig. 2 PRL-3-sensitive ezrin dephosphorylation in response to TiO_2 exposure in vitro and in vivo. **A** Immunoblot analysis of total EZR and pEZR in BEAS-2B cells pretreated with a PRL-3 inhibitor prior to TiO_2 exposure. **B** Densitometric quantification of pEZR and total EZR levels normalized to β-actin. $n = 5$ per group. **C** Immunoblot analysis of total EZR and pEZR following siRNA-mediated knockdown of PRL-3 in BEAS-2B cells exposed to TiO_2 or SiO_2 particles. **D** Representative immunofluorescence images of lung tissue sections from control mice and TiO_2-treated mice in the presence of PRL-3 inhibitor. EZR and pEZR were detected in separate tissue sections using FITC-conjugated secondary antibodies. Merged images show FITC (green) and nuclear staining with DAPI (blue). Scale bar = 20 μm. **E** Quantification of pEZR fluorescence intensity normalized to DAPI following PRL-3 inhibition. $n = 4$ per group. **F** Representative immunofluorescence images of lung tissue sections from control mice and TiO2-treated mice in the presence of PRL-3 siRNA. EZR and pEZR were detected in separate tissue sections using FITC-conjugated secondary antibodies. Merged images show FITC (green) and nuclear staining with DAPI (blue). Scale bar = 20 μm. **G** Quantification of pEZR fluorescence intensity normalized to DAPI following PRL-3 silencing. $n = 4$ per group. Data are presented as mean ± SD for in vitro experiments, and shown as individual data points with median and interquartile range (IQR) for in vivo experiments

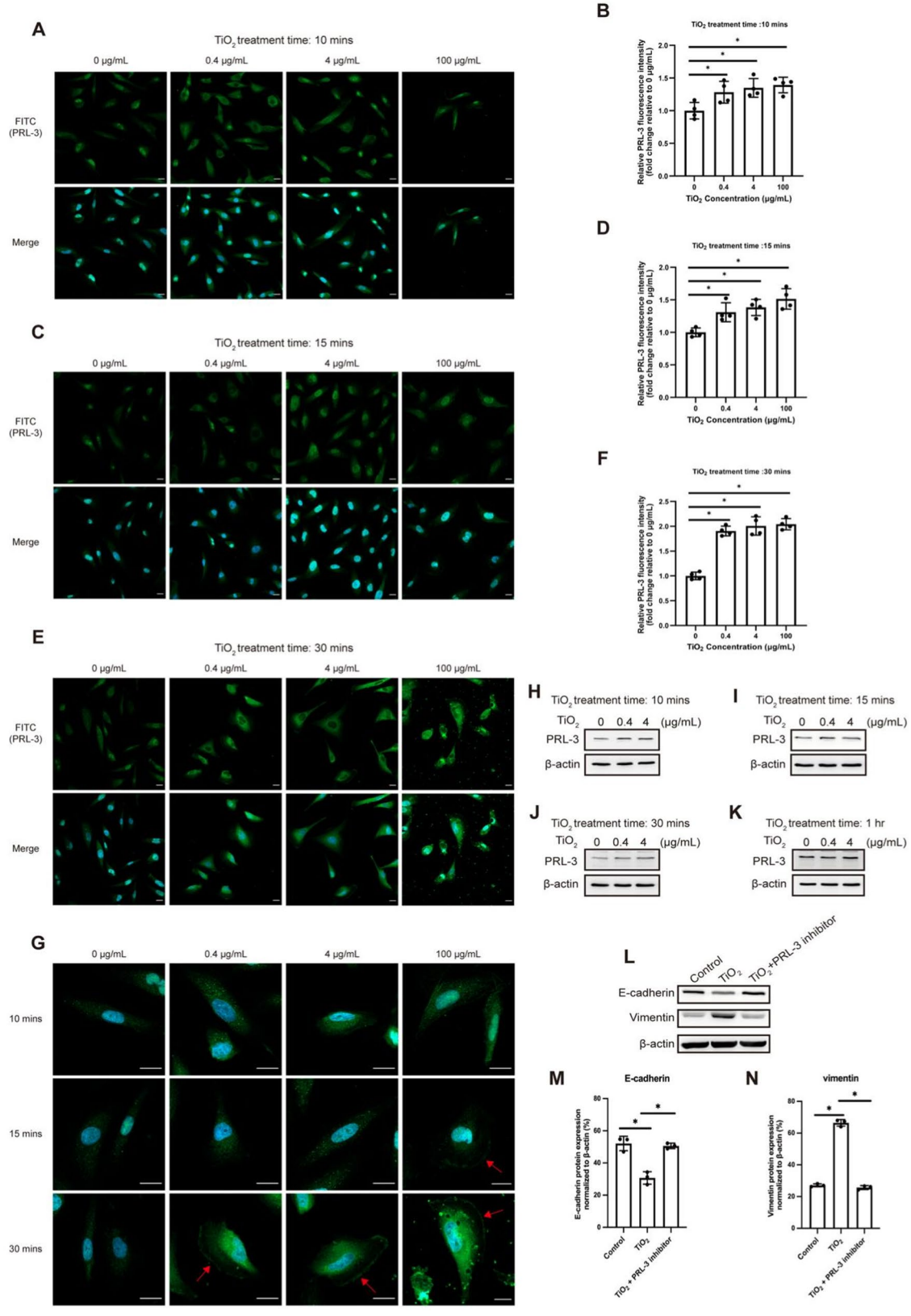

Fig. 3 (See legend on next page.)

(See figure on previous page.)

Fig. 3 TiO_2 exposure induces transient PRL-3 upregulation and membrane relocalization associated with epithelial remodeling. **A**, **C**, **E** Representative immunocytochemical images showing PRL-3 localization in BEAS-2B cells after TiO_2 exposure for 10, 15, and 30 min at the indicated concentrations. PRL-3 was visualized using FITC (green), and nuclei were counterstained with DAPI (blue). Scale bar = 20 μm. **B**, **D**, **F** Quantification of PRL-3 fluorescence intensity normalized to DAPI. $n = 4$ per group. **G** High-magnification images highlighting membrane-associated PRL-3 signals (arrows), derived from **A**, **C**, and **E**. Scale bar = 20 μm. **H–K** Representative immunoblot images showing PRL-3 protein signals at early time points in BEAS-2B cells following TiO_2 exposure at the indicated concentrations. **L** Immunoblot analysis of E-cadherin and vimentin in BEAS-2B cells following TiO_2 exposure with or without PRL-3 inhibitor. **M**, **N** Densitometric quantification of E-cadherin and vimentin levels normalized to β-actin. $n = 3$ per group. Data are presented as mean ± SD. $^*p < 0.05$

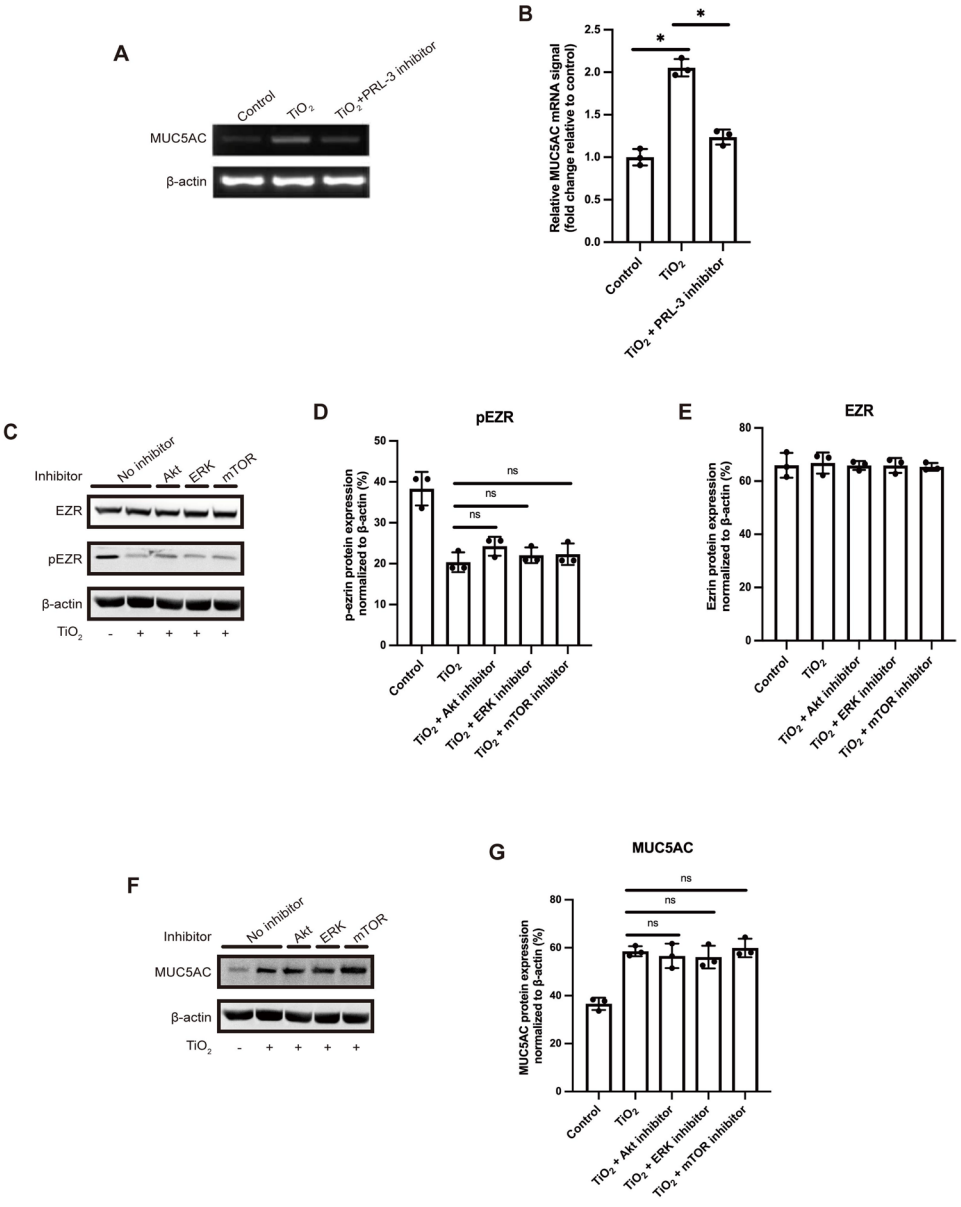

Fig. 4 PRL-3–sensitive ezrin dephosphorylation occurs independently of canonical Akt, ERK, and mTOR signaling. **A** Representative semi-quantitative RT-PCR gel image showing MUC5AC mRNA expression following TiO_2 exposure with or without PRL-3 inhibitor. **B** Densitometric quantification of MUC5AC mRNA signal normalized to β-actin. $n = 3$ per group. **C** Immunoblot analysis of total EZR and pEZR in BEAS-2B cells pretreated with Akt, ERK, or mTOR inhibitors prior to TiO_2 exposure. "No inhibitor" indicates TiO_2-treated cells without inhibitor pretreatment. **D**, **E** Densitometric quantification of pEZR and total EZR levels normalized to β-actin. $n = 3$ per group. **F** Immunoblot analysis of MUC5AC protein levels in BEAS-2B cells following TiO_2 exposure in the presence of Akt, ERK, or mTOR inhibitors. "No inhibitor" indicates TiO_2-treated cells without inhibitor pretreatment. **G** Densitometric quantification of MUC5AC protein levels normalized to β-actin. $n = 3$ per group. Data are presented as mean ± SD. $^*p < 0.05$; ns, not significant

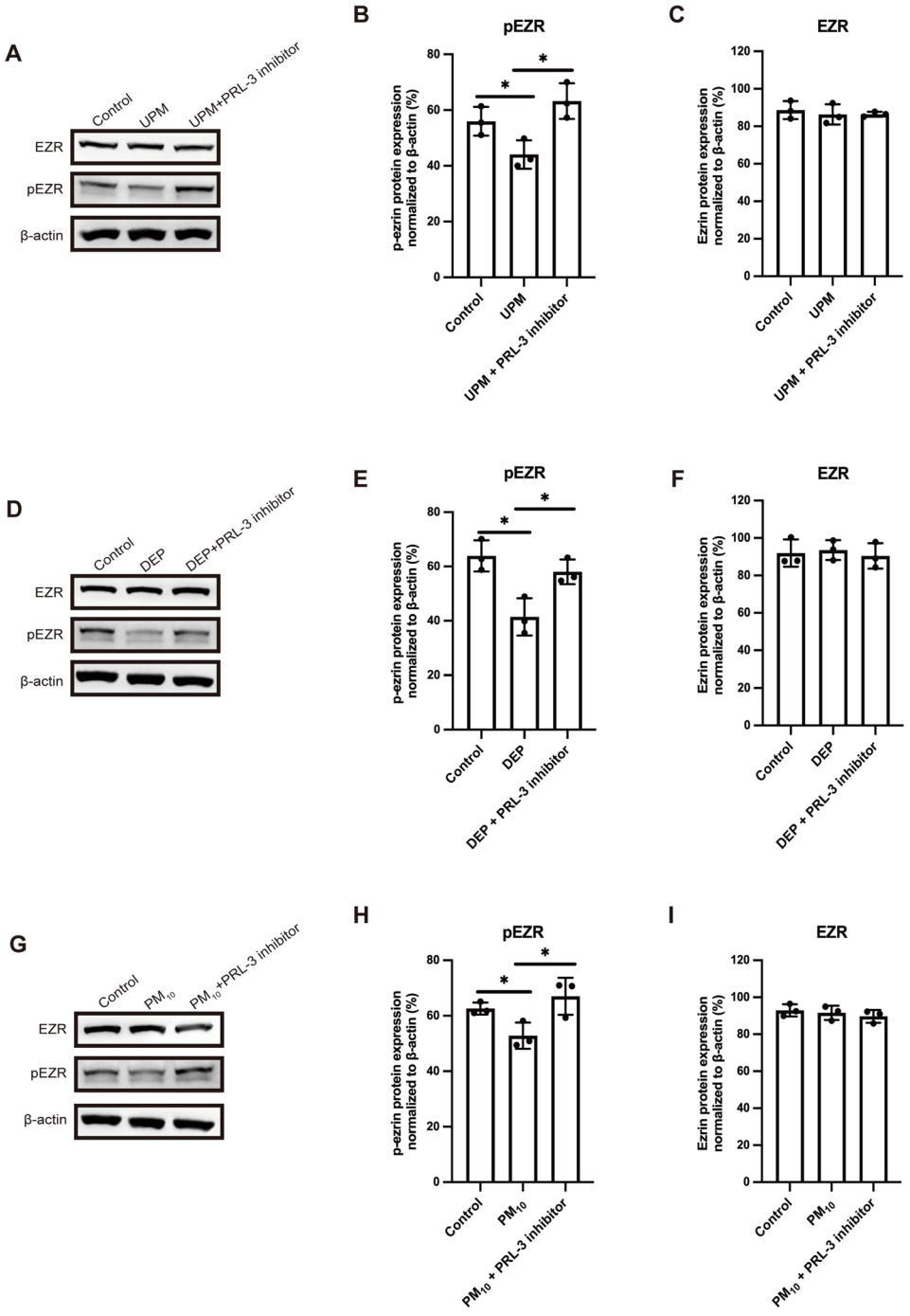

Fig. 5 PRL-3-sensitive ezrin dephosphorylation across environmentally relevant particulate matter types. **A–I** Immunoblot analysis and densitometric quantification of pEZR and total EZR levels in BEAS-2B cells following exposure to urban particulate matter (UPM) **A–C**, diesel exhaust particle (DEP) **D–F**, or PM_{10} **G–I**, in the presence or absence of PRL-3 inhibitor, normalized to β-actin. $n = 3$ per group. Data are presented as mean ± SD. *$p < 0.05$

phosphoproteomic profiling (Table 1). Within this network, PRL-3 was identified as a phosphatase-associated regulatory mediator associated with PRL-3-sensitive ezrin dephosphorylation and downstream cytoskeleton-associated epithelial responses, including EMT-associated marker changes and MUC5AC upregulation (Fig. 6).

Discussion

In this study, we identify a cytoskeleton-centered molecular response linking particulate exposure to early airway epithelial alterations [1, 2, 31]. Using an unbiased phosphoproteomic approach under non-cytotoxic exposure conditions, we found that particulate exposure preferentially engages phosphorylation-dependent signaling

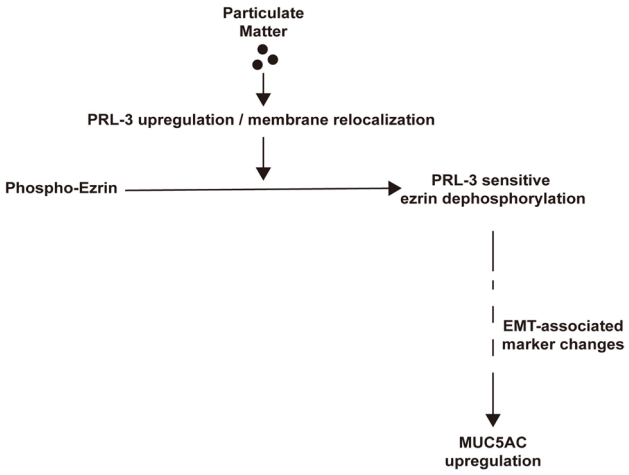

Fig. 6 Proposed model of PRL-3-sensitive early cytoskeletal signaling in particulate-induced airway epithelial responses. Schematic illustration summarizing the proposed model in which acute particulate matter exposure is associated with PRL-3 upregulation and membrane relocalization, together with PRL-3-sensitive ezrin dephosphorylation, leading to cytoskeleton-associated epithelial responses, EMT-associated marker changes, and MUC5AC upregulation

networks associated with membrane–cytoskeleton coupling and epithelial structural integrity [15, 16, 32]. TiO_2 was selected as a compositionally defined model particle to reduce the physicochemical heterogeneity inherent to ambient PM and to enable focused analysis of early particle-induced cytoskeletal signaling under controlled acute exposure conditions. This approach was intended to identify molecular initiating events rather than to fully reproduce real-world airborne PM exposure. To address the environmental relevance of this pathway, we further examined particulate matter types that are present in airborne environments, including UPM, DEP, and PM_{10}. The observation that these environmentally relevant particulates also induced PRL-3-sensitive ezrin dephosphorylation supports the relevance of this cytoskeletal response beyond the TiO_2 model system. Within this early signaling context, protein tyrosine phosphatase PRL-3 emerged as a phosphatase-associated regulatory mediator linked to PRL-3-sensitive ezrin dephosphorylation and cytoskeleton-associated epithelial responses, including EMT-associated marker changes and MUC5AC upregulation.

A central finding of this study is the identification of an early signaling axis that precedes canonical inflammatory and stress responses. While PM-induced oxidative stress and cytokine-driven inflammation have been extensively characterized [6–8], these processes typically represent downstream events following epithelial injury. Our findings instead support a model in which particulate exposure rapidly perturbs cytoskeleton-associated signaling pathways, suggesting that cytoskeleton-associated epithelial alterations may represent early initiating events in airway pathology [9, 33].

This concept is consistent with emerging models in which early epithelial structural alterations and barrier-related signaling contribute to the initiation of airway disease [34]. PRL-3 has been extensively studied in cancer biology as a regulator of cytoskeletal dynamics, membrane organization, and cell motility [35–37]. Our findings extend this framework by identifying PRL-3 as an early environmentally responsive phosphatase in airway epithelial cells. Acute particulate exposure induces rapid and transient PRL-3 upregulation accompanied by membrane relocalization, events that occur within minutes and precede both cytotoxicity and overt epithelial remodeling.

Functional inhibition and genetic suppression experiments consistently showed that PRL-3 blockade restored particulate-induced ezrin dephosphorylation, supporting its role as a phosphatase-associated regulatory mediator in this early cytoskeletal response. This stepwise approach, from phosphoproteomic screening of ERM family alterations to targeted validation of ezrin and PRL-3, supports the functional involvement of PRL-3 in particulate-induced ezrin dephosphorylation. In addition, the SiO_2 result from the siRNA experiment provided further support that PRL-3-sensitive ezrin dephosphorylation is not restricted to TiO_2. Because SiO_2 was used as a supporting particulate comparison, this finding was interpreted as complementary evidence for a broader particle-associated cytoskeletal response. Ezrin plays a central role in maintaining epithelial architecture by linking cortical actin to the plasma membrane, and its phosphorylation at Thr567 is required for its active conformation [38–40]. The PRL-3-sensitive ezrin dephosphorylation observed in this study may alter membrane–cytoskeleton coupling, thereby providing a molecular basis for epithelial remodeling-associated responses, including EMT-associated molecular changes and mucin overproduction [41–43].

Importantly, inhibition of canonical Akt, ERK, or mTOR signaling pathways failed to prevent ezrin dephosphorylation or MUC5AC upregulation, supporting the involvement of a PRL-3-sensitive cytoskeletal response distinct from these canonical signaling pathways. These findings support the presence of a non-canonical signaling pathway linking particulate exposure to structural epithelial remodeling.

The observation of PRL-3-sensitive ezrin dephosphorylation across multiple particulate types, including urban particulate matter, diesel exhaust particles, and PM_{10}, further suggests that this cytoskeleton-associated response is not restricted to the TiO_2 model system. Such early signaling responses may contribute to molecular initiating events associated with environmentally induced airway epithelial injury [9, 33].

From a translational perspective, the identification of an early, non-inflammatory signaling mechanism has important implications. Our findings raise the possibility that proximal signaling regulators such as PRL-3 may represent potential targets for preserving epithelial integrity following particulate exposure, although this will require further validation in clinically relevant models.

Several limitations should be considered. While acute exposure models are useful for identifying early signaling events, they do not fully recapitulate chronic environmental exposure. The in vitro experiments were performed primarily in BEAS-2B cells, which are useful for mechanistic studies but may not fully reflect the biological properties of primary human airway epithelial cells. Future studies incorporating primary airway epithelial models, TEER measurements, permeability assays, and tight junction analyses will help define how PRL-3-sensitive ezrin dephosphorylation contributes to functional epithelial barrier integrity. In addition, the in vivo findings were limited to female mice, and several experiments were performed with modest sample sizes, particularly the in vivo analyses; therefore, future studies with larger cohorts including both sexes will further strengthen the generalizability of the observations. Direct assessment of PRL-3 protein knockdown efficiency in lung tissues, validation of PRL-3 inhibitor selectivity under in vivo exposure conditions, and measurement of PRL-3 enzymatic activity will further refine the interpretation of PRL-3-sensitive airway epithelial responses. It will also be important to determine how this pathway interacts with immune responses during the development of airway disease.

Conclusion

In summary, our findings identify a PRL-3-sensitive cytoskeletal signaling axis as an early molecular mechanism linking particulate matter exposure to molecular alterations associated with early airway epithelial responses. These results provide mechanistic insight into the initiation of pollutant-associated airway injury and suggest that PRL-3 may represent a potential target for further investigation.

Abbreviations

Akt	Protein kinase B
ANOVA	Analysis of variance
BEAS-2B	Human bronchial epithelial cells
DEP	Diesel exhaust particles
EMT	Epithelial–mesenchymal transition
ERK	Extracellular signal-regulated kinase
ERM	Ezrin-radixin-moesin
EZR	Ezrin
IQR	Interquartile range
MUC5AC	Mucin 5AC
mTOR	Mechanistic target of rapamycin
pEZR	Phosphorylated ezrin
PM	Particulate matter
PM_{10}	Particulate matter with an aerodynamic diameter of ≤ 10 μm
PRL-3	Phosphatase of regenerating liver-3
PTP4A3	Protein tyrosine phosphatase 4A3
SD	Standard deviation
siRNA	Small interfering RNA
SiO_2	Silicon dioxide
TiO_2	Titanium dioxide
UPM	Urban particulate matter

Supplementary Information

The online version contains supplementary material available at https://doi.org/10.1186/s12931-026-03834-9.

Supplementary Material 1.

Supplementary Material 2.

Supplementary Material 3.

Acknowledgements

Not applicable.

Authors' contributions

H.Y. and M.C. contributed equally to this work and share first authorship. H.Y.: cell-based experiments, investigation, methodology, data analysis and interpretation, validation, and writing - original draft. M.C.: animal experiments, investigation, methodology, and data analysis and interpretation. Y.H.: data analysis and interpretation (LC-ESI-MS/MS), Experimental support (cell-based assays). J.A.: Experimental support (animal experiments). A.-S.J.: clinical expertise (respiratory medicine), interpretation of airway pathology-related features, and analysis of airway tissue data. S.-K.L.: conceptual input, overall organization and revision of the manuscript. T.R.: conceptualization, methodology, writing - review and editing, validation, funding acquisition, and supervision. All authors read and approved the final manuscript.

Funding

This research was supported by Basic Science Research Program of the National Research Foundation of Korea (NRF) funded by the Ministry of Education (Republic of Korea) (Grant No. 2017R1A2B4012007).

Data availability

All data generated or analysed during this study are included in this published article and its supplementary information files.

Declarations

Ethics approval and consent to participate

All animal experiments were approved by the Institutional Animal Care and Use Committee (IACUC) of Hanyang University (Approval number: HY-IACUC-25-0227).

Consent for publication

Not applicable.

Competing interests

The authors declare no competing interests.

Author details

[1]Department of Bioengineering, College of Engineering, Hanyang University, 222 Wangsimni-ro, Seongdong-gu, Seoul 04763, Republic of Korea
[2]Department of Internal Medicine, Soonchunhyang University Bucheon Hospital, Bucheon 14584, Republic of Korea
[3]Institute of Bioengineering and Biopharmaceutical Research, Hanyang University, Seoul 04763, Republic of Korea

Received: 31 March 2026 / Accepted: 14 July 2026
Published online: 22 July 2026

References

1. Pope CA 3rd, Dockery DW. Health effects of fine particulate air pollution: lines that connect. J Air Waste Manag Assoc. 2006;56:709–42.
2. Kelly FJ, Fussell JC. Air pollution and airway disease. Clin Exp Allergy. 2011;41:1059–71.
3. Holt PG, Strickland DH. Interactions between innate and adaptive immunity in asthma pathogenesis: new perspectives from studies on acute exacerbations. J Allergy Clin Immunol. 2010;125:963–72. quiz 973 – 964.
4. Whitsett JA, Alenghat T. Respiratory epithelial cells orchestrate pulmonary innate immunity. Nat Immunol. 2015;16:27–35.
5. Crystal RG, Randell SH, Engelhardt JF, Voynow J, Sunday ME. Airway epithelial cells: current concepts and challenges. Proc Am Thorac Soc. 2008;5:772–7.
6. Li N, Xia T, Nel AE. The role of oxidative stress in ambient particulate matter-induced lung diseases and its implications in the toxicity of engineered nanoparticles. Free Radic Biol Med. 2008;44:1689–99.
7. Donaldson K, Stone V, Seaton A, MacNee W. Ambient particle inhalation and the cardiovascular system: potential mechanisms. Environ Health Perspect. 2001;109(Suppl 4):523–7.
8. Zhou H, Kobzik L. Effect of concentrated ambient particles on macrophage phagocytosis and killing of Streptococcus pneumoniae. Am J Respir Cell Mol Biol. 2007;36:460–5.
9. Xing YF, Xu YH, Shi MH, Lian YX. The impact of PM2.5 on the human respiratory system. J Thorac Dis. 2016;8:E69–74.
10. Reid CE, Brauer M, Johnston FH, Jerrett M, Balmes JR, Elliott CT. Critical Review of Health Impacts of Wildfire Smoke Exposure. Environ Health Perspect. 2016;124:1334–43.
11. Cooper DM, Loxham M. Particulate matter and the airway epithelium: the special case of the underground? Eur Respir Rev. 2019;28:190066. https://doi.org/10.1183/16000617.0066-201.
12. Holgate ST, Lackie PM, Davies DE, Roche WR, Walls AF. The bronchial epithelium as a key regulator of airway inflammation and remodelling in asthma. Clin Exp Allergy. 1999;29(Suppl 2):90–5.
13. Heijink IH, Brandenburg SM, Postma DS, van Oosterhout AJ. Cigarette smoke impairs airway epithelial barrier function and cell-cell contact recovery. Eur Respir J. 2012;39:419–28.
14. Gonzalez-Mariscal L, Tapia R, Chamorro D. Crosstalk of tight junction components with signaling pathways. Biochim Biophys Acta. 2008;1778:729–56.
15. Bretscher A, Edwards K, Fehon RG. ERM proteins and merlin: integrators at the cell cortex. Nat Rev Mol Cell Biol. 2002;3:586–99.
16. Fehon RG, McClatchey AI, Bretscher A. Organizing the cell cortex: the role of ERM proteins. Nat Rev Mol Cell Biol. 2010;11:276–87.
17. Olsen JV, Mann M. Status of large-scale analysis of post-translational modifications by mass spectrometry. Mol Cell Proteom. 2013;12:3444–52.
18. Needham EJ, Parker BL, Burykin T, James DE, Humphrey SJ. Illuminating the dark phosphoproteome. Sci Signal. 2019;12(565):eaau8645. https://doi.org/10.1126/scisignal.aau8645.
19. Zeng Q, Si X, Horstmann H, Xu Y, Hong W, Pallen CJ. Prenylation-dependent association of protein-tyrosine phosphatases PRL-1, -2, and – 3 with the plasma membrane and the early endosome. J Biol Chem. 2000;275:21444–52.
20. Bessette DC, Qiu D, Pallen CJ. PRL PTPs: mediators and markers of cancer progression. Cancer Metastasis Rev. 2008;27:231–52.
21. Al-Aidaroos AQ, Zeng Q. PRL-3 phosphatase and cancer metastasis. J Cell Biochem. 2010;111:1087–98.
22. Byun J, Song B, Lee K, Kim B, Hwang HW, Ok MR, Jeon H, Lee K, Baek SK, Kim SH, et al. Identification of urban particulate matter-induced disruption of human respiratory mucosa integrity using whole transcriptome analysis and organ-on-a chip. J Biol Eng. 2019;13:88.
23. Lee KW, Nam MH, Lee HR, Hong CO, Lee KW. Protective effects of chebulic acid on alveolar epithelial damage induced by urban particulate matter. BMC Complement Altern Med. 2017;17:373.
24. Baarsma HA, Van der Veen C, Lobee D, Mones N, Oosterhout E, Cattani-Cavalieri I, Schmidt M. Epithelial 3D-spheroids as a tool to study air pollutant-induced lung pathology. SLAS Discov. 2022;27:185–90.
25. Lasagni Vitar RM, Tau J, Reides CG, Berra A, Ferreira SM, Llesuy SF. Evaluation of Oxidative Stress Markers in Human Conjunctival Epithelial Cells Exposed to Diesel Exhaust Particles (DEP). Invest Ophthalmol Vis Sci. 2015;56:7058–66.
26. Somayajulu M, Wright R, Muhammed F, McClellan SA, Ibrahim A, Hazlett LD. PM(10) dysregulates epithelial barrier function in human corneal epithelial cells that is restored by antioxidant SKQ1. Toxicol Appl Pharmacol. 2024;492:117122.
27. Fujii T, Hayashi S, Hogg JC, Vincent R, Van Eeden SF. Particulate matter induces cytokine expression in human bronchial epithelial cells. Am J Respir Cell Mol Biol. 2001;25:265–71.
28. Forte E, Orsatti L, Talamo F, Barbato G, De Francesco R, Tomei L. Ezrin is a specific and direct target of protein tyrosine phosphatase PRL-3. Biochim Biophys Acta. 2008;1783:334–44.
29. Sung HJ, Ahn JM, Yoon YH, Rhim TY, Park CS, Park JY, Lee SY, Kim JW, Cho JY. Identification and validation of SAA as a potential lung cancer biomarker and its involvement in metastatic pathogenesis of lung cancer. J Proteome Res. 2011;10:1383–95.
30. Heo SH, Lee SJ, Ryoo HM, Park JY, Cho JY. Identification of putative serum glycoprotein biomarkers for human lung adenocarcinoma by multilectin affinity chromatography and LC-MS/MS. Proteomics. 2007;7:4292–302.
31. Holgate ST. The airway epithelium is central to the pathogenesis of asthma. Allergol Int. 2008;57:1–10.
32. McClatchey AI. ERM proteins at a glance. J Cell Sci. 2014;127:3199–204.
33. Donaldson K, Brown D, Clouter A, Duffin R, MacNee W, Renwick L, Tran L, Stone V. The pulmonary toxicology of ultrafine particles. J Aerosol Med. 2002;15:213–20.
34. Heijink IH, Nawijn MC, Hackett TL. Airway epithelial barrier function regulates the pathogenesis of allergic asthma. Clin Exp Allergy. 2014;44:620–30.
35. Zeng Q, Dong JM, Guo K, Li J, Tan HX, Koh V, Pallen CJ, Manser E, Hong W. PRL-3 and PRL-1 promote cell migration, invasion, and metastasis. Cancer Res. 2003;63:2716–22.
36. Rios P, Li X, Kohn M. Molecular mechanisms of the PRL phosphatases. FEBS J. 2013;280:505–24.
37. Gari HH, DeGala GD, Ray R, Lucia MS, Lambert JR. PRL-3 engages the focal adhesion pathway in triple-negative breast cancer cells to alter actin structure and substrate adhesion properties critical for cell migration and invasion. Cancer Lett. 2016;380:505–12.
38. Matsui T, Maeda M, Doi Y, Yonemura S, Amano M, Kaibuchi K, Tsukita S, Tsukita S. Rho-kinase phosphorylates COOH-terminal threonines of ezrin/radixin/moesin (ERM) proteins and regulates their head-to-tail association. J Cell Biol. 1998;140:647–57.
39. Gautreau A, Louvard D, Arpin M. Morphogenic effects of ezrin require a phosphorylation-induced transition from oligomers to monomers at the plasma membrane. J Cell Biol. 2000;150:193–203.
40. Fievet BT, Gautreau A, Roy C, Del Maestro L, Mangeat P, Louvard D, Arpin M. Phosphoinositide binding and phosphorylation act sequentially in the activation mechanism of ezrin. J Cell Biol. 2004;164:653–9.
41. Thiery JP, Acloque H, Huang RY, Nieto MA. Epithelial-mesenchymal transitions in development and disease. Cell. 2009;139:871–90.
42. Kalluri R, Weinberg RA. The basics of epithelial-mesenchymal transition. J Clin Invest. 2009;119:1420–8.
43. Rogers DF. Physiology of airway mucus secretion and pathophysiology of hypersecretion. Respir Care. 2007;52:1134–46. discussion 1146 – 1139.

Publisher's note

Springer Nature remains neutral with regard to jurisdictional claims in published maps and institutional affiliations.